Sensitivity of Atmospheric Radiative Heating Rate Profiles to Variations of Cloud Layer Overlap

TING CHEN*

Department of Earth and Environmental Sciences, Columbia University, New York, New York

YUANGCHONG ZHANG

Department of Applied Physics and Applied Mathematics, Columbia University, New York, New York

WILLIAM B. ROSSOW

NASA Goddard Institute for Space Studies, New York, New York

(Manuscript received 9 November 1998, in final form 29 September 1999)

ABSTRACT

Three different cloud overlap schemes are applied to the International Satellite Cloud Climatology Project (ISCCP) vertical distribution of clouds in the radiative transfer model from the National Aeronautics and Space Administration Goddard Institute for Space Studies climate GCM to study the sensitivity of radiative fluxes and atmospheric radiative heating rate profiles to variations in cloud vertical structure. This study differs from previous ones because the ISCCP dataset constrains the total column optical thickness of the clouds at each location, a fact that is used to constrain cloud overlap occurrence. Moreover, this study considers the effects of cloud vertical structure on both shortwave (SW) and longwave (LW) fluxes at the top of the atmosphere, at the surface, and in the atmosphere. The in-atmosphere net fluxes are decomposed further into vertical profiles of radiative heating and cooling rates. The results show that the changes in the top-of-atmosphere (TOA) and surface (SRF) radiative fluxes vary among the different schemes, depending on the part of the atmosphere–surface system and spectral band (SW and LW) considered, but that the magnitudes of the changes generally are small. The scheme without a total optical thickness constraint produces opposite-signed changes in fluxes (except for the SRF LW flux) and the profile of atmospheric radiative heating rate in comparison with the schemes with the constraint. The constraint on total optical thickness eliminates nearly all of the effects on the total TOA and SRF radiation budget, significantly reducing the frequency of layer overlap occurrence and thereby reducing the effect of overlap on the radiative heating rate profiles. Even when the assumptions are changed to produce a frequency of occurrence of multilayer clouds that is similar to other estimates, the resulting changes in the radiative heating rate profile are quantitatively small. The magnitude of these changes is similar to the magnitude of the total overall cloud effect, however, making the layer overlap critical to accurate determinations of the shape of the radiative heating rate profiles.

1. Introduction

Much effort has been devoted to investigating how clouds affect the global radiative heating of the earth, but the focus has been on cloud-induced changes of the top-of-atmosphere (TOA) and/or the surface radiation budgets (Barkstrom 1984; Harrison et al. 1990; Rossow and Lacis 1990; Hartmann et al. 1992; Ockert-Bell and Hartmann 1992; Darnell et al. 1992; Rossow and Zhang 1995). A few studies have examined cloud effects on the general circulation through their modification of the radiative heating profile within the atmosphere (e.g., Freeman and Liou 1979; Slingo and Slingo 1988; Randall et al. 1989; Wang and Rossow 1998). Currently available satellite analyses provide accurate information on cloud-top heights, with some systematic errors, especially for optically thin cirrus (cf. Minnis et al. 1993; Liao et al. 1995b), but they do not provide any direct information on cloud-base heights and generally assume that all clouds are single layers.[1] Thus, calculations of

*Current affiliation: Department of Applied Physics and Applied Mathematics, Columbia University, New York, New York.

Corresponding author address: Dr. Ting Chen, Dept. of Applied Physics and Applied Mathematics, Columbia University, 2880 Broadway, New York, NY 10025.
E-mail: tchen@giss.nasa.gov

[1] Some algorithms have been proposed to detect an optically thin, high-level cloud layer over a low-level cloud layer using multispectral methods (Baum et al. 1994; Jin and Rossow 1997).

© 2000 American Meteorological Society

radiative fluxes that use the same assumption together with climatological values of cloud layer thicknesses show a negative bias in the downwelling longwave flux at the surface because the average cloud-base altitude is too high (Zhang et al. 1995; Rossow and Zhang 1995). The main reason for this bias is that an estimate of cloud-base height based on cloud-top height and layer thicknesses does not account for the occurrence of multilayered clouds, which often are observed (Warren et al. 1985; Wang and Rossow 1995; Wang 1997).

With the mean atmospheric temperature distribution established by the interaction of total diabatic heating and the atmospheric circulation, net radiative cooling under clear conditions serves to stabilize the troposphere. Relative to the earth's surface, however, the radiative cooling of the troposphere creates instability and induces convection. Cloud modifications of this situation are complex, depending on the height and vertical structure of the clouds. For example, Ramaswamy and Ramanathan (1989) show that the longwave heating rate within cirrus anvil clouds can range from a large cooling when they overlie optically thick clouds to a large heating when no other clouds are below. Wang and Rossow (1998) illustrate more effects of cloud-top height variations and the occurrence of two-layered clouds. Some situations in their study (for example, moving a single-layer cloud below the original global mean location or inserting a lower cloud layer below a cloud layer at the top of troposphere) tend to destabilize the atmosphere and enhance moist convection.

General circulation model studies have formulated this problem in terms of parameterizations of subgrid-scale cloud layer overlap in their radiation schemes, because these models generally predict cloud fractions in each model layer independently without explicitly specifying the relative geometry among multiple cloud layers (Liang and Wang 1997; Morcrette and Fouquart 1986; Stubenrauch et al. 1997). Some studies confirm that the radiation is sensitive to the cloud overlap assumption used (Kuhn 1978; Stubenrauch et al. 1997). The current study of cloud layer overlap effects differs from previous ones[2] by considering both shortwave and longwave fluxes at the top of the atmosphere, at the surface, and in the atmosphere; by considering radiative heating profiles; and by exploiting an extra piece of information provided by the International Satellite Cloud Climatology Project (ISCCP; Rossow and Schiffer 1991) cloud dataset. In addition to providing the distribution of cloud-top locations, ISCCP also reports the total column cloud optical thicknesses. This extra information provides a strong constraint on simple cloud layer overlap schemes that reduces the magnitude of its effect.

In section 2, after describing the radiative transfer model and datasets used in the calculations, we consider several constrained versions of the simple overlap assumptions that have been suggested by observations (cf. Warren et al. 1985; Tian and Curry 1989) and also their unconstrained forms. Section 3 briefly examines the degree to which changing cloud overlap alters the calculated surface and TOA radiative fluxes and the total in-atmosphere net radiative fluxes. In section 4 we illustrate the effects of these different cloud overlap assumptions on the calculated radiative heating rate profiles. Implications are discussed in section 5.

2. Radiative transfer model, cloud dataset, and cloud layer overlap schemes

a. Radiative transfer model

The radiative transfer model used in these calculations is a modified version of the Goddard Institute for Space Studies GCM (Hansen et al. 1983). The model includes a detailed, spectrally dependent treatment of surface reflection and emission, atmospheric gaseous absorptions, and scattering by both gases and clouds [see Zhang et al. (1995) for more details] to calculate upwelling and downwelling, shortwave (SW; wavelengths 0.2–5.0 μm) and longwave (LW; wavelengths 5.0–200 μm) fluxes, and layer heating rates as a function of atmospheric pressure. Although the cloud properties are obtained from the ISCCP D1 dataset (see next section), which reports both ice and liquid water clouds, all clouds in the flux calculation model are considered to be liquid water as in Zhang et al. (1995). This assumption has the primary effect of underestimating the scattering and absorption of SW by upper-level clouds by about 10% (relative), because the retrieved optical thickness of ice-phase clouds usually is smaller for the same visible reflectance than it is for liquid droplet clouds, but the scattering and absorption are slightly larger for the same optical thickness (Mishchenko et al. 1996; Ho et al. 1998). Longwave fluxes are less sensitive to differences in phase and particle size. The model does not include the longwave scattering by clouds. This omission mainly affects the results for thin cirrus clouds in the infrared window region (Liou 1986; Toon et al. 1989; Fu et al. 1997), because the scattering effect of clouds is generally small in the longwave. All these biases are not as important when examining sensitivity to vertical structure changes, because our comparisons are made relative to single-layer calculations using the same assumptions. For the purpose of this study, the model is adjusted to allow for more than one cloud layer to occur in a column according to the fractional areal coverage determined by the satellite observations together with the overlap assumptions described below. All radiative fluxes are calculated first for each com-

[2] T. P. Charlock (1999, personal communication) considered the effects of random or maximum cloud layer overlap assumptions on surface longwave fluxes and longwave cooling rate profile of the atmosphere using the ISCCP cloud dataset.

bination of vertical structure, assuming complete overcast, and for clear sky (whether there is any or not) and then are averaged together, weighted by the actual area fractions, to obtain the total flux profiles. The vertical divergences of shortwave and longwave fluxes in each layer of the atmosphere also are determined this way to give the shortwave heating rate and the longwave cooling rate profiles.

b. Cloud dataset

The global distributions of surface, atmosphere, and cloud properties are taken from the ISCCP D1 dataset (Rossow et al. 1996) supplemented by other datasets as needed [see Zhang et al. (1995) for a more complete description of all the datasets used]. The ISCCP D1 product is a revision of the C1 product (Rossow and Schiffer 1991) to improve cirrus detection and property retrievals and to give more complete cloud-type information. The cloud properties, including cloud-cover fraction (C_f), cloud-top pressure (P_c) and temperature (T_c), and cloud optical thickness (τ), and water path, are available every 3 h at 280-km resolution over the whole globe. In addition to the area-average cloud parameters within each map grid box, the distribution of cloud parameters is reported also in terms of 15 cloud types, defined by three intervals of cloud-top pressure, three optical thickness categories, and the phases of the cloud particles. Because cloud optical thicknesses are determined from visible radiance measurements, which are available only during daytime, and the cloud-top temperature is more accurately determined as a function of optical thickness (Rossow et al. 1996), nighttime cloud-type information is refined by interpolating between daytime cloud observations to complete the diurnal cycle. The interpolation procedure involves two steps, as follows. 1) The nighttime values of optical thickness and top temperature for individual cloud types are set to the nearest corresponding daytime values. 2) The relative proportions of the individual cloud types within each pressure category during daytime are used to scale the nighttime cloud fraction for the same pressure category (if no measurement of nighttime total cloud fraction is available, the fractions of each nighttime cloud type are set equal to the corresponding values of nearest daytime observation). Missing daytime observations occasionally are filled in the same way. For the map grid boxes that have no cloud observations for the whole day (e.g., in the polar regions in some seasons), no calculations are performed.

The computational resources available for this study precluded calculations that cover extensive periods of time. Because this study is intended to examine only the sensitivity of radiative fluxes and atmospheric heating rate profiles to variations in cloud vertical structures, with emphasis on the consequences of violating the conservation of vertically integrated cloud optical thickness, we perform calculations on only 4 days of data. Because the magnitude of the cloud radiative effects also depends on the properties of the surface and atmosphere, particularly their seasonal variations, and on the seasonal variation of solar insolation, however, we choose 4 specific days (1 from each season) from the D1 dataset to provide a representative sample of the large-scale variations of cloud properties, surface and atmospheric temperatures, humidity, and solar zenith angles: 15 January, 15 April, 15 July, and 15 October 1991.

For simplicity, we combine the 15 cloud types into 3 cloud types: low, middle, and high (low cloud is defined by cloud-top pressure $P_c > 680$ mb, middle cloud by $440 < P_c \leq 680$ mb, and high cloud by $P_c \leq 440$ mb); average optical thicknesses and top temperatures are determined with a radiative weighting (cf. Rossow et al. 1996). Cloud-base pressures are determined from cloud-top pressures for the three cloud types using a climatology of cloud layer thickness, which is a function of cloud-top height, latitude, and season based on rawinsonde and surface observations (Poore et al. 1995; Wang and Rossow 1995).

c. Cloud layer overlap schemes

Satellite observations from above the clouds report only the cloud-top pressure of the first cloud layer encountered going downward from the top of the atmosphere.[3] The ISCCP cloud statistics are determined assuming no cloud layer overlap; that is, the cloud amounts at each level are the actual amounts seen by the satellite. For example, if high-level cloud cover is complete, zero cloud amounts at lower levels will be reported. To obtain a better vertical distribution of cloud layers from the satellite results, we can try simple cloud layer overlap rules that have been suggested by observations: random overlap (Warren et al. 1985) and a mix of random and maximum overlap (Tian and Curry 1989). Note that such an approach cannot work if the dataset represents too small a sample to include some indication of the cloud layers actually present. For example, if the area considered is too small, the likelihood of detecting more than one cloud layer is reduced. For the ISCCP map gridbox size, about 75% of all boxes detect the presence of at least two cloud layers. The opposite extreme of the original ISCCP statistics is to assume maximum overlap, meaning that detected lower-level clouds are assumed to be present below any detected upper-level clouds. Random overlap and the mixed random–maximum overlap will produce results that are intermediate between maximum and no overlap, so we consider only maximum and random overlap as

[3] Surface observations have a similar problem with a bottom-up view, but the climatology reported by Warren et al. (1986, 1988) alters the estimates of upper-level cloud amounts by using a kind of random overlap assumption.

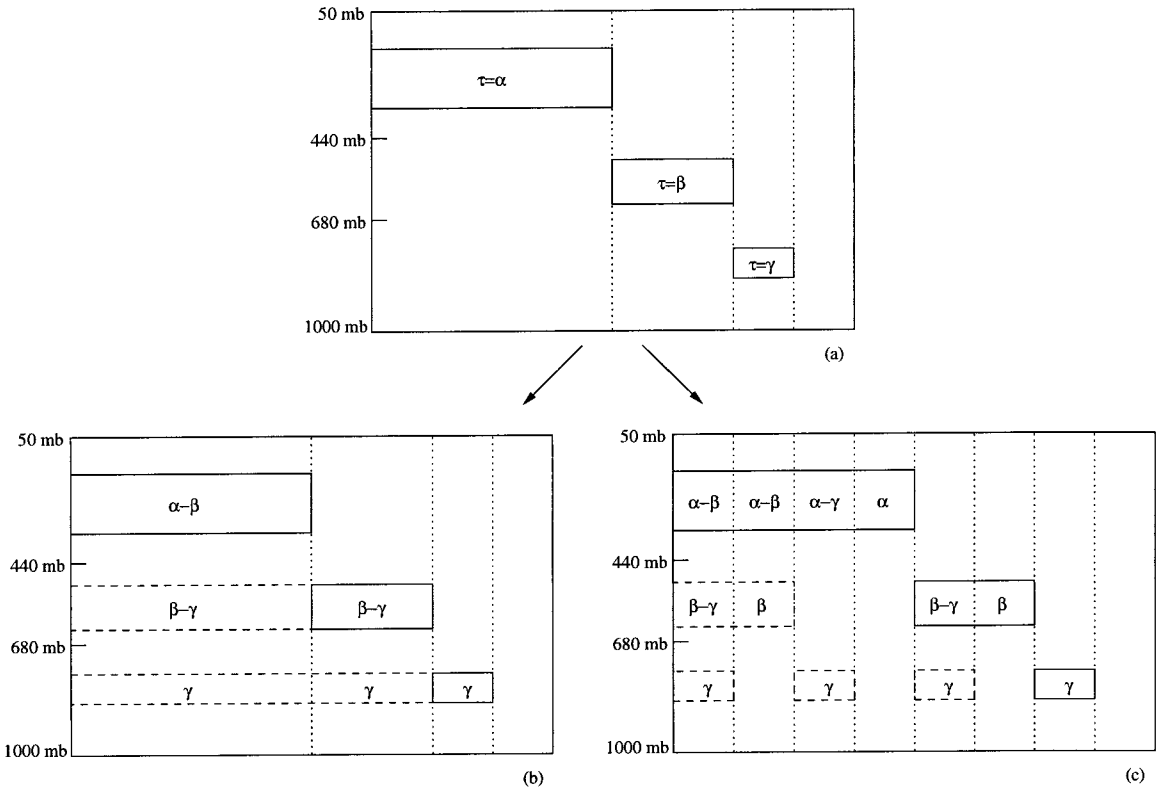

FIG. 1. Schematic showing how the constraint-I overlap scheme changes the cloud vertical distribution within a model grid box. In this figure, α, β, and γ denote the optical thicknesses of the high-, mid-, and low-level cloud, respectively, where $\alpha \geq \beta + \tau_{\text{threshold}}$ and $\beta \geq \gamma + \tau_{\text{threshold}}$. (a) Before overlap, (b) after overlap using maximum rule, and (c) after overlap using random rule.

compared with no overlap. Because we do not know whether such an approach is correct, our only purpose is to test how sensitive the radiative fluxes and heating rate profiles are to different cloud layer overlap schemes.

If two cloud layers are present in a D1 grid box, maximum overlap requires all of the upper-level cloud to be underlain by the lower-level cloud, so the area fraction of lower-level cloud is increased by an amount equal to the amount of upper-level cloud (cf. Fig. 1b). For random overlap, the total amount of lower-level cloud is renormalized to the fraction of the total area actually observed. For example, if the observed upper-level and lower-level cloud fractions are C_u and C_l, defined in terms of the total area, then the fraction of the lower level that is actually seen is $1 - C_u$. The lower-level cloud fraction then is increased to $C_l/(1 - C_u)$. Thus, the amount of lower-level cloud underlying the upper-level cloud is given by $C_l C_u/(1 - C_u)$ (cf. Fig. 1c).

If we use no other information, then maximum and random overlap constitute a set, referred to as the ''no constraint'' set. Using the total column cloud optical thickness observed by ISCCP as a constraint on the allowed overlaps defines two other sets, called ''constraint I'' and ''constraint II.'' Thus, we have seven overlap schemes: no overlap, random or maximum overlap with no constraint, random or maximum overlap with constraint I, and random or maximum overlap with constraint II.

The idea behind the constraint-I scheme is very simple. If there are two cloud layers occurring simultaneously in one map grid box (280 km in size), and the optical thickness of the lower-level cloud is larger than that of the upper-level cloud, then the upper-level cloud could not be the result of an optically thinner cloud overlying a similar lower-level cloud. For this result to be true, the optical thickness of the upper-level cloud must exceed that of the lower-level cloud. Thus, in the constraint-I scheme, overlapping of cloud layers that occur together, whether random or maximum, is not allowed unless the optical thickness of the upper-level cloud exceeds that of the lower-level cloud by at least a prescribed positive threshold value $\tau_{\text{threshold}}$. This optical thickness constraint limits the number of map grid boxes in which cloud overlapping occurs, becoming a more restrictive limit as the threshold value increases (e.g., on average, cloud overlap occurs in about 45% of all boxes when $\tau_{\text{threshold}} = 0.01$ and in about 38% of all boxes when $\tau_{\text{threshold}} = 0.5$ at any given measurement time). If overlap is allowed, then the fractional area of the lower-level cloud that underlies the upper-level cloud is determined by either a random or maximum

overlap rule as before. The cloud-top temperature and optical thickness of the underlying cloud layer are the same as the observed lower-level clouds, consistent with the assumption determining the constraint. The top temperature of the upper-level cloud with a cloud below is as observed, and its optical thickness then is set to $\tau_{\text{upper}} - \tau_{\text{lower}}$ to conserve total optical thickness. The properties of the single-layer clouds are the same as observed directly. Figure 1 illustrates how the maximum and random constraint-I overlap schemes work for a map grid box with $\tau_{\text{high cloud}} \geq \tau_{\text{middle cloud}} + \tau_{\text{threshold}}$ and $\tau_{\text{middle cloud}} \geq \tau_{\text{low cloud}} + \tau_{\text{threshold}}$. With the maximum overlap rule, a map grid box observed to contain three cloud layers together (for simplicity, this is the maximum possible) can be divided into four partitions, namely, one partition with only one cloud layer, one partition with two overlapping cloud layers, one partition with all the three cloud layers overlapping each other, and a clear-sky partition, if there is any (Fig. 1b). For random overlap, there can be eight partitions corresponding to different vertical distributions of cloud layers, namely, three partitions with only one cloud layer each, three partitions with two overlapping cloud layers, one partition with all three cloud layers overlapping each other, and a clear-sky partition (Fig. 1c). Note that this scheme differs from that used by Ridout and Rosmond (1996) and others, because layer overlap is constrained to conserve vertically integrated cloud optical thickness.

The constraint-II scheme allows overlapping of two cloud layers observed together whenever the optical thickness of the upper-level cloud exceeds a prescribed minimum value $\tau_{\text{threshold}}$. In this case, the upper-level cloud optical thickness need not be larger than that of the lower-level cloud. This optical thickness constraint also limits (but to a lesser degree in comparison with the constraint-I scheme as long as the $\tau_{\text{threshold}}$ is less than the average optical thickness value of the lower-level clouds) the number of map grid boxes in which cloud overlapping occurs, becoming a more restrictive limit as the threshold value increases (e.g., on average, cloud overlap occurs in about 75% of all boxes when $\tau_{\text{threshold}} = 0.01$ and in about 70% of all boxes when $\tau_{\text{threshold}} = 0.5$ at any given time). For that part of the upper-level cloud that is underlain by a lower-level cloud, the optical thickness of the upper cloud is set to $\tau_{\text{threshold}}$ and the top temperature is as observed. The optical thickness of the underlying cloud layer then is set to $\tau_{\text{upper}} - \tau_{\text{threshold}}$ to conserve total optical thickness; the top temperature of the lower layer is as observed. The fraction of the upper-level cloud with another layer below is determined by either a maximum or random overlap rule as described above.

The no-constraint scheme, which allows overlap (either random or maximum) whenever two (or more) cloud layers occur together in the same map grid box (on average, this happens in about 75% of all boxes at any one time, as mentioned before) and without regard to conserving total optical thickness, maximizes the frequency of overlap possible with the ISCCP dataset and illustrates the consequences of violating the conservation of cloud optical thickness, as some investigators have done. In this scheme the overlapping cloud layers retain the same cloud optical thickness and top temperature values as are observed. This approach systematically increases the total cloud optical thickness.

TABLE 1. Summary of experiments discussed in the text.

Experiment	Description
MEAN	Radiative fluxes are computed once for the mean cloud properties (C_f, τ, and T_c)
TYPE9	Radiative fluxes are computed separately for each of the nine ISCCP cloud types (cirrus, cirrostratus, deep convective, altocumulus, altostratus, nimbostratus, cumulus, stratocumulus, stratus), and the results are averaged linearly to obtain the total fluxes
TYPE3	Radiative fluxes are computed separately for each of the three cloud types (high, middle, and low cloud) then linearly averaged
1C0.5RAN	Overlap experiment using constraint-I scheme and random rule with $\tau_{\text{threshold}}$ of 0.5. Radiative fluxes are computed separately for each different distribution of the cloud layers, and the results are averaged linearly to obtain the total fluxes
1C0.01RAN	Constraint-I scheme, random rule with $\tau_{\text{threshold}}$ of 0.01
1C0.5MAX	Constraint-I scheme, maximum rule with $\tau_{\text{threshold}}$ of 0.5
1C0.01MAX	Constraint-I scheme, maximum rule with $\tau_{\text{threshold}}$ of 0.01
2C0.5RAN	Constraint-II scheme, random rule with $\tau_{\text{threshold}}$ of 0.5
2C0.01RAN	Constraint-II scheme, random rule with $\tau_{\text{threshold}}$ of 0.01
2C0.5MAX	Constraint-II scheme, maximum rule with $\tau_{\text{threshold}}$ of 0.5
2C0.01MAX	Constraint-II scheme, maximum rule with $\tau_{\text{threshold}}$ of 0.01
NCRAN	No-constraint scheme, random rule
NCMAX	No-constraint scheme, maximum rule

Table 1 summarizes the experiments performed with all of these overlap schemes to test the sensitivity of the radiative fluxes and heating rate profiles to the assumed cloud vertical structure. Although none of these overlap schemes is completely justifiable from observations of the actual cloud layers (Tian and Curry's result is based on observations for one location and season: midlatitude winter ocean), these schemes do cover the whole possible range of changes in lower-level cloud amounts that are consistent with the surface observations, providing a meaningful estimate of the sensitivity of the radiation to cloud vertical structure.

Figure 2 shows the global frequency, averaged over all 4 days, of single-layer, two-layer, and three-layer clouds produced by the three overlap schemes, using both random and maximum rules, together with the 5-yr (1991–95) climatological, global mean frequency determined from rawinsonde profiles of humidity (Wang 1997). In the case of the τ-constrained overlaps, the

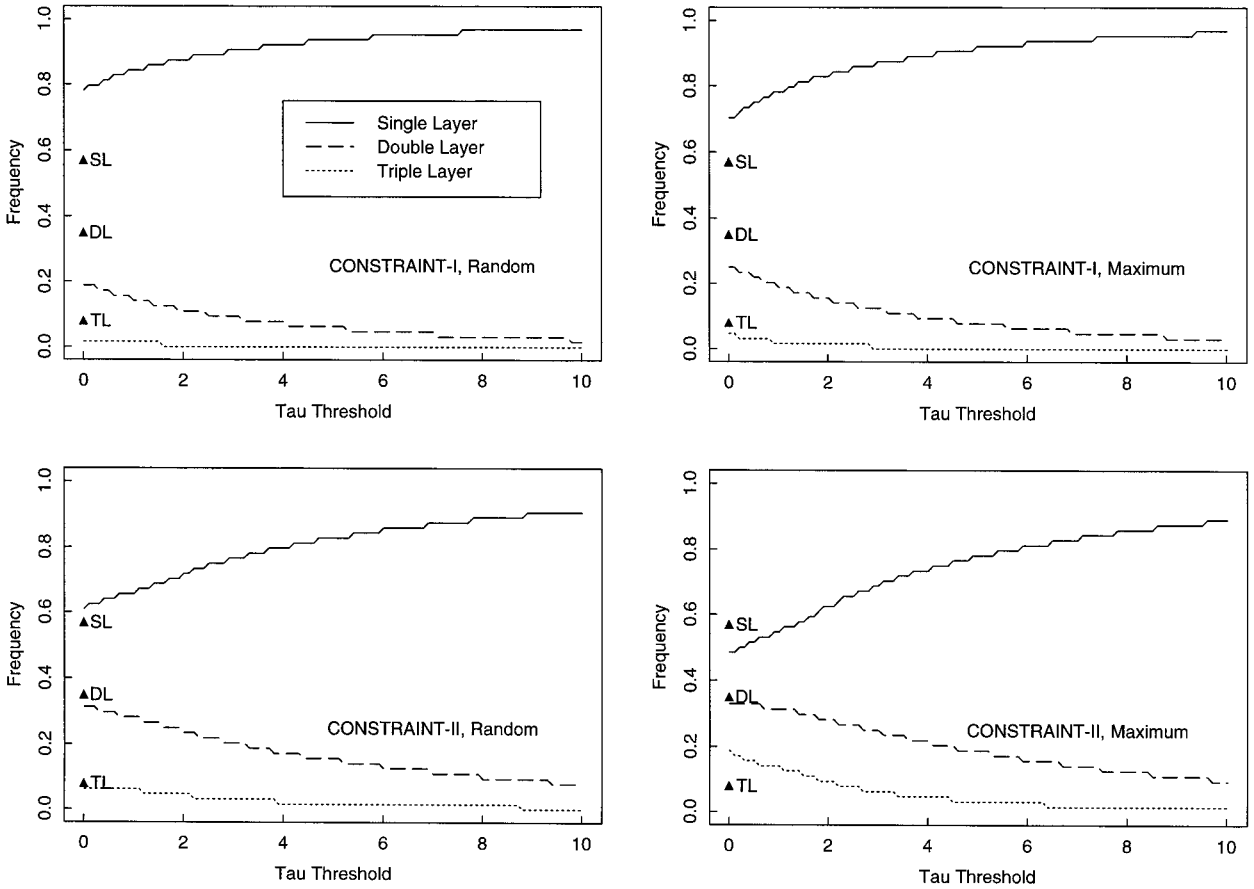

FIG. 2. Global ''annual'' (4-day average) mean frequency of single-layer (SL), double-layer (DL), and triple-layer (TL) clouds produced by each group of overlap schemes as a function of $\tau_{\text{threshold}}$. Solid triangles denote the corresponding frequencies from rawinsonde analysis (Wang 1997).

results are shown as a function of the value of $\tau_{\text{threshold}}$; the no-constraint case is equivalent to $\tau_{\text{threshold}} = 0$ using the constraint-II scheme, and the nonoverlap case gives a single-layer frequency of 1.0. As expected, larger values of $\tau_{\text{threshold}}$ reduce the frequency of multilayered clouds. Comparison of these frequencies with those determined from rawinsonde profiles of humidity shows that smaller values of $\tau_{\text{threshold}}$ yield the better agreement. Maximum constraint I with $\tau_{\text{threshold}} = 0.01$ (1C0.01MAX) underestimates the frequency of multilayered clouds (defined as multilayered cloud fraction normalized by total cloud fraction), yielding 30% as compared with 43% from the rawinsonde data.[4] The maximum no-constraint experiment (NCMAX) and the equivalent maximum constraint-II experiment with $\tau_{\text{threshold}} = 0.01$ (2C0.01MAX) overestimate the frequency of multilayered cloud (52% as compared with 43%), however, as does the maximum constraint-II experiment with $\tau_{\text{threshold}} = 0.5$ (2C0.5MAX) (48% as compared with 43%). Because most experiments underestimate the global frequency of multilayered clouds in comparison with those determined from rawinsonde profiles of humidity, we isolate those locations where cloud structure changes (i.e., those map grid boxes where cloud overlap occurs) rather than looking at global or even zonal mean changes. In other words, unchanged locations are excluded from the averages unless otherwise noted.

Figure 3 compares the 4-day-averaged, zonal mean, mid-, and low-layer cloud amounts obtained from ISCCP by using two of the overlap schemes with the mid- and low-layer cloud amounts based on surface observations (Warren et al. 1986, 1988), also illustrating the sensitivity to the value of $\tau_{\text{threshold}}$. The constraint-I scheme (either random or maximum, $\tau_{\text{threshold}} = 0.01$) produces the best match to the latitude variations of the surface-based low-level cloud amounts but generally underestimates the midlevel cloud amount slightly (Fig. 3a). Use of a larger value of $\tau_{\text{threshold}}$ (not shown) increases the differences, producing underestimates of

[4] Note that our number (43%) is slightly less than the number (46%) that appeared in Wang (1997), because we treat a multilayer cloud formed from the cloud layers within the same height category as a single-layer cloud for consistency with our overlap schemes.

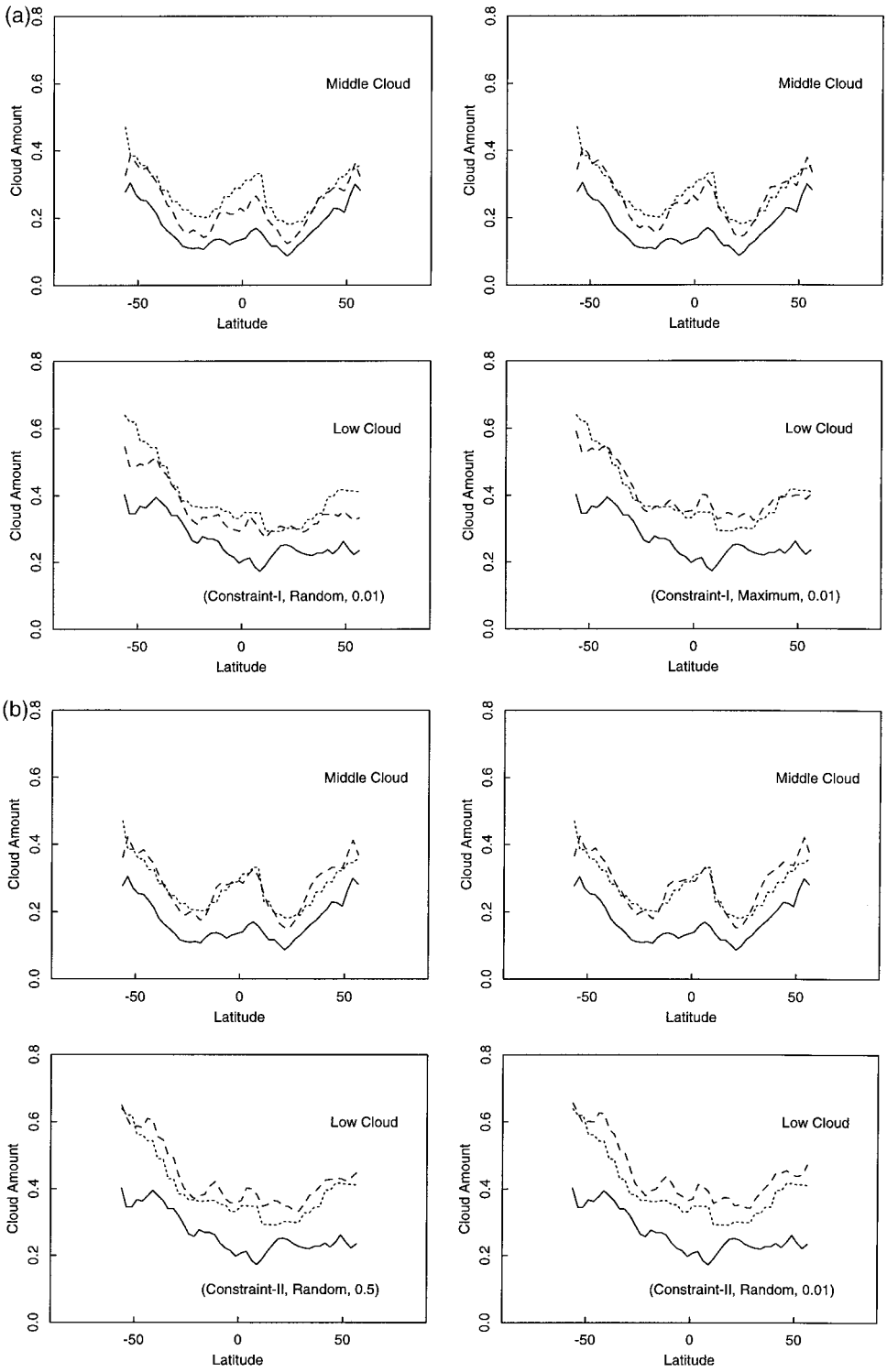

FIG. 3. (a) Comparison of zonal mean, middle, and low cloud amount between ISCCP (before and after overlap) and surface observations. Left panels are for experiment 1C0.01RAN, right panels are for experiment 1C0.01MAX. Solid line: ISCCP cloud amount before overlap (4-day average); long-dashed line: ISCCP cloud amount after overlap (4-day average); short-dashed line: 30-yr (1952–81) average of surface observations. (b) Same as (a) but for experiments 2C0.5RAN (left panels) and 2CO.01RAN (right panels).

both low-level and midlevel cloud amounts. The random constraint-II scheme (for $0.5 \geq \tau_{\text{threshold}} \geq 0.01$) produces a better match for midlevel cloud amounts but overestimates low-level cloud amounts (Fig. 3b). The maximum constraint-II scheme (not shown) overestimates both low-level and midlevel cloud amounts for $0.5 \geq \tau_{\text{threshold}} \geq 0.01$ by much larger amounts. Nevertheless, all of these comparisons show that the layer cloud amounts produced by applying these different schemes to the ISCCP D1 dataset are in a sufficiently realistic range to evaluate the importance of cloud layer structure on the radiation budget. Also, note that the ISCCP high-cloud amounts agree well with the surface observed high-cloud amounts (not shown), with a mean difference less than 0.01 and rms error of ~0.04 (although both datasets actually underestimate high-cloud amounts for different reasons; cf. Rossow et al. 1993; Liao et al. 1995a; Jin et al. 1996; Stubenrauch et al. 1999; Wang et al. 2000).

3. Sensitivity of cloud radiative effects to variations in the cloud layer overlap

In this section we consider the sensitivity of the cloud radiative effect (CRE = total sky minus clear sky) on fluxes at TOA, the surface (SRF), and in the atmosphere (ATM = TOA minus SRF) to changes in the assumed vertical structure of the clouds. By comparing fluxes obtained using the overlap assumptions described above with those obtained using a treatment with single-layer clouds and no overlap (e.g., Darnell et al. 1992; Zhang et al. 1995), we can estimate possible errors produced by neglecting the vertical structure of the clouds. Figure 4 and Tables 2–4 summarize the global mean changes of the SW and LW CREs for all the overlap experiments relative to the reference nonoverlap counterpart (TYPE3). Figure 4 shows the averages of only changed locations for each individual day; Tables 2–4 show the global 4-day averages of both changed locations and all locations. For the daily mean calculation, a map grid box is considered to be a changed location as long as cloud overlap occurs in at least one out of the eight times per day. Thus, a large portion of all boxes are considered to be changed locations, for example, 61%–67% in the constraint-I experiments and 85%–90% in the constraint-II and no-constraint experiments. Also shown are the changes in the fluxes produced by calculating the fluxes with a separate treatment of nine cloud types (TYPE9), as in a companion paper (Chen et al. 2000), instead of a single-average cloud layer (MEAN) as done by Zhang et al. (1995). Because the day-to-day variation of the flux changes is small (Fig. 4), the numbers cited in the text below are 4-day-averaged results (unless otherwise indicated).

a. Top of atmosphere

For the SW CRE at TOA (Fig. 4 and Table 2), the overlap experiments using the constraint-I scheme (1C0.5RAN to 1C0.01MAX) cause slightly more sunlight to be absorbed by the earth–atmosphere system in comparison with the nonoverlap counterpart (TYPE3); global mean differences range from 0.6 to 0.9 W m^{-2} (0.3–0.6 W m^{-2}) for changed (all) locations. This magnitude is about the same as the effect of treating individual cloud types (TYPE9 or TYPE3) as compared with an average single cloud layer (MEAN). The overlap experiments using the constraint-II scheme (2C0.5RAN to 2C0.01MAX) have a similar but larger effect, ranging from 1.7 to 2.4 W m^{-2} (1.4–2.2 W m^{-2}) for changed (all) locations. This change arises for both τ-conserving overlap schemes (constraint-I and constraint-II) because they both reduce (by different amounts) the optical thickness of the high-level clouds, although preserving the total optical thickness, which allows more SW to be absorbed by water vapor at lower levels. In fact, this effect is enhanced by increased low-level clouds that reflect some of the photons upward, back through overlying water vapor; two cloud layers would also increase the number of photons that pass through the intervening water vapor layer more than twice. This fact explains the greater increase of absorbed SW in the constraint-II experiments, because this overlap scheme reduces the upper-level optical thicknesses more than does constraint-I. Without a constraint on total optical thickness (the no-constraint schemes, NCRAN and NCMAX), creating overlapping clouds increases the total optical thickness and diminishes the absorbed SW radiation at TOA by 9.9 and 14.6 W m^{-2} (8.9 and 13.1 W m^{-2}, about 20% of the global mean TOA SW CRE) for changed (all) locations. Thus, changing the cloud vertical structure while conserving the total cloud optical thickness produces only very small changes in the TOA net SW fluxes, but, if cloud overlapping is done without conservation of total optical thickness, significant (and opposite signed, as compared with the τ-conserving overlap schemes) errors in the TOA SW flux will be introduced.

For the LW CRE at TOA (Fig. 4 and Table 2), τ-conserving overlap schemes increase the LW radiation loss from the earth–atmosphere system (i.e., decrease the TOA LW CRE); however, the constraint-I scheme causes only small changes, from 1.7 to 3.3 W m^{-2} (1.0–2.3 W m^{-2}) for changed (all) locations, whereas the constraint-II scheme causes much larger changes, from 6.8 to 11.8 W m^{-2} (5.7–10.7 W m^{-2}) for changed (all) locations. Again, the effect can be explained by the thinning of the high-level clouds when τ is conserved with layer overlaps, allowing more LW radiation to escape to space from the lower atmosphere. The larger changes in the constraint-II experiments arise from the small values of $\tau_{\text{threshold}}$, which correspond to small LW emissivities (e.g., $\tau = 0.5$ is equivalent to an emissivity of about 0.2 at 11-μm wavelength). The changes in LW CRE at TOA without an optical thickness constraint (NCRAN and NCMAX) are much smaller (0.9 and 1.6 W m^{-2} for changed locations, 0.8 and 1.4 W m^{-2} for

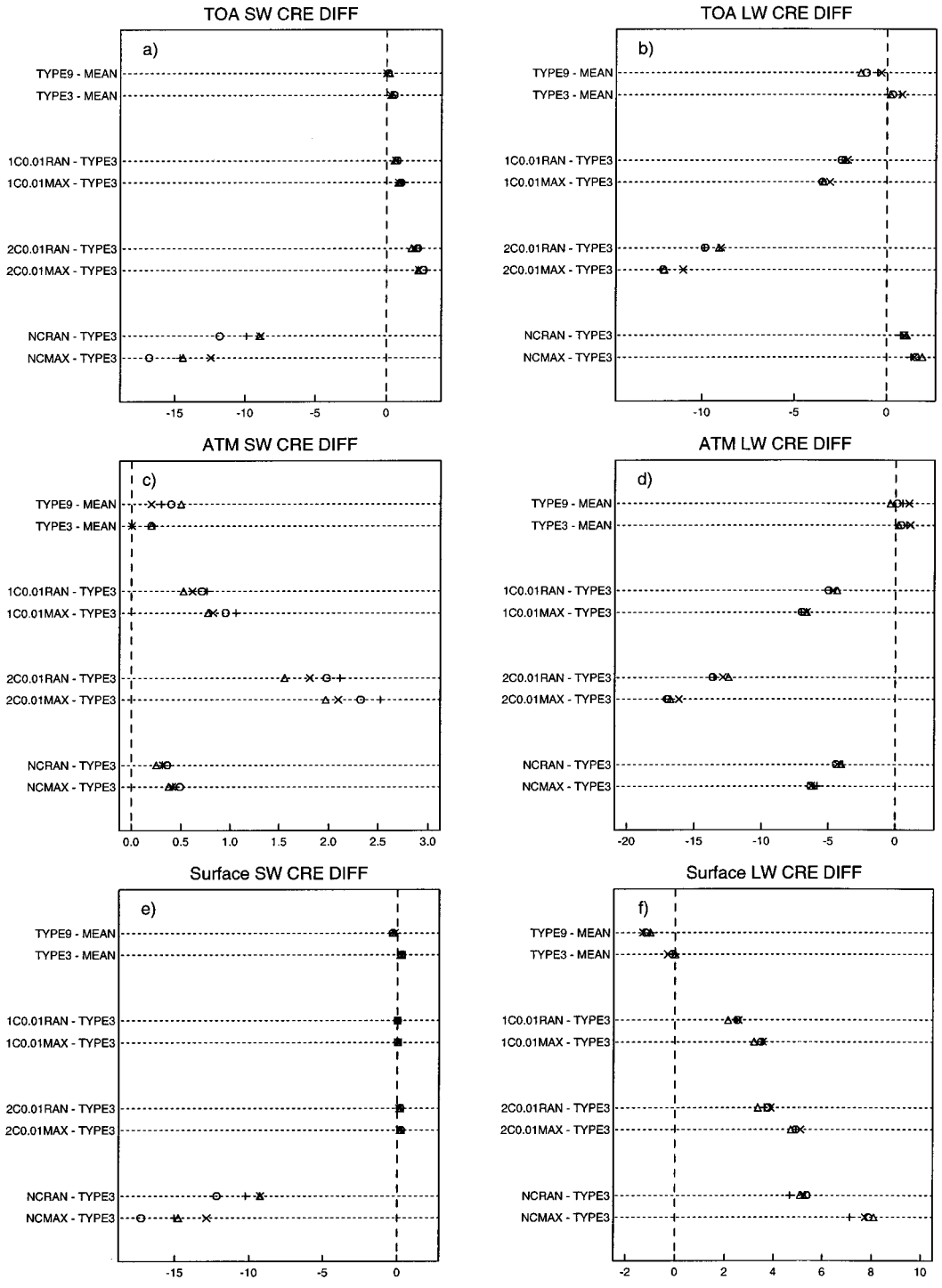

FIG. 4. Global mean CRE differences (W m^{-2}) between the six overlap experiments and the nonoverlap counterpart (TYPE3) (overlap minus nonoverlap; unchanged locations excluded), together with the CRE differences between two nonoverlap experiments (TYPE9 and TYPE3) and an experiment using the mean cloud properties (MEAN) (nonoverlap minus MEAN; all locations). (a) SW CRE at TOA, (b) LW CRE at TOA, (c) SW CRE in the atmosphere, (d) LW CRE in the atmosphere, (e) SW CRE at the surface, and (f) LW CRE at the surface. Individual daily results (○: 15 Jan 1991; △: 15 Apr 1991; +: 15 Jul 1991; ×: 15 Oct 1991) are shown here.

TABLE 2. Global annual (4-day averaged) mean differences and their standard deviations (in parentheses) of the calculated shortwave (SW), longwave (LW), and total (TL, i.e., SW plus LW) cloud radiative effects (CRE; W m^{-2}) at TOA between various experiments (for both changed locations and all locations).

	Changed			All		
CRE at TOA	SW	LW	TL	SW	LW	TL
TYPE9 − MEAN	—	—	—	0.0 (1.0)	−0.8 (2.6)	−0.8 (2.5)
TYPE3 − MEAN	—	—	—	0.4 (0.7)	0.5 (2.4)	0.9 (2.2)
1C0.5RAN − TYPE3	0.6 (0.9)	−1.7 (2.9)	−1.1 (2.3)	0.3 (0.7)	−1.0 (2.4)	−0.7 (1.9)
1C0.01RAN − TYPE3	0.7 (1.0)	−2.3 (3.9)	−1.6 (3.1)	0.5 (0.9)	−1.5 (3.4)	−1.0 (2.7)
1C0.5MAX − TYPE3	0.8 (1.1)	−2.4 (3.6)	−1.6 (2.9)	0.5 (0.9)	−1.5 (3.1)	−1.0 (2.4)
1C0.01MAX − TYPE3	0.9 (1.2)	−3.3 (4.9)	−2.4 (4.0)	0.6 (1.1)	−2.3 (4.3)	−1.7 (3.5)
2C0.5RAN − TYPE3	1.7 (2.4)	−6.8 (9.3)	−5.1 (7.3)	1.4 (2.3)	−5.7 (8.9)	−4.3 (7.0)
2C0.01RAN − TYPE3	2.0 (2.8)	−9.4 (12.7)	−7.4 (10.3)	1.8 (2.7)	−8.5 (12.3)	−6.7 (10.1)
2C0.5MAX − TYPE3	2.0 (2.5)	−8.3 (10.1)	−6.3 (8.1)	1.7 (2.4)	−7.1 (9.8)	−5.4 (7.8)
2C0.01MAX − TYPE3	2.4 (2.9)	−11.8 (14.0)	−9.4 (11.5)	2.2 (2.8)	−10.7 (13.7)	−8.5 (11.3)
NCRAN − TYPE3	−9.9 (11.8)	0.9 (1.3)	−9.0 (11.2)	−8.9 (11.6)	0.8 (1.3)	−8.1 (10.9)
NCMAX − TYPE3	−14.6 (14.6)	1.6 (2.0)	−13.0 (13.6)	−13.1 (14.5)	1.4 (2.0)	−11.7 (13.5)

all locations), because the optical thicknesses of the higher-level clouds are unchanged, and the addition of lower-level cloud underneath has little effect on the TOA LW fluxes.

b. Surface

Figure 4 also shows the global mean differences of CREs at the surface between the various overlap experiments and the reference nonoverlap case (see also Table 3). As with the SW CRE at TOA, the surface SW CRE for the τ-conserving experiments is virtually unchanged when various amounts of cloud layer overlap are introduced. Because the cloud optical thicknesses are kept constant, the small changes are associated with the changing relationship of the cloud layers and the water vapor. On the other hand, without the τ-constraint (NCRAN and NCMAX), increased total cloud optical thickness, produced by overlapping layers, markedly reduces the net surface SW by 10.2 and 15.0 W m^{-2} (9.2 and 13.5 W m^{-2}) for changed (all) locations.

All the overlap experiments produce increases of the surface LW CRE in comparison with the nonoverlap case (TYPE3), ranging from only 2.3 W m^{-2} (1.4 W m^{-2}) in 1C0.5RAN to 7.7 W m^{-2} (7.0 W m^{-2}) in NCMAX for changed (all) locations. This increase results directly from the increase in low- and midlevel cloud cover, producing lower average cloud-base heights in the overlap experiments. This effect is larger over land than over ocean, because the overlap schemes produce a relatively larger change in low- and midlevel clouds over land for which there was much less to begin with (Fig. 5), and because higher humidity (both relative and absolute) at the surface of the ocean reduces the effect of lowering the cloud bases.

c. In atmosphere

The in-atmosphere CRE is given by the difference between the TOA and surface CREs, providing an indication of how clouds affect the radiation budget of the entire atmospheric column from TOA to surface. Introducing cloud overlap increases the in-atmosphere SW CRE by only 0.3 W m^{-2} (0.3 W m^{-2}) in NCRAN to 2.2 W m^{-2} (2.0 W m^{-2}) in 2C0.01MAX for changed (all) locations (Fig. 4 and Table 4); this small range is sufficient to change the sign of the in-atmosphere SW CRE from negative to positive, however. As the amount

TABLE 3. Same as Table 2 but at the surface.

	Changed			All		
CRE at the surface	SW	LW	TL	SW	LW	TL
TYPE9 − MEAN	—	—	—	−0.3 (1.0)	−1.1 (1.9)	−1.4 (2.0)
TYPE3 − MEAN	—	—	—-	0.3 (0.4)	−0.1 (1.2)	0.2 (1.2)
1C0.5RAN − TYPE3	0.0 (0.1)	2.3 (3.3)	2.3 (3.3)	0.0 (0.1)	1.4 (2.8)	1.4 (2.8)
1C0.01RAN − TYPE3	0.0 (0.1)	2.4 (3.4)	2.4 (3.4)	0.0 (0.1)	1.7 (3.0)	1.7 (3.0)
1C0.5MAX − TYPE3	0.0 (0.1)	3.3 (4.2)	3.3 (4.2)	0.0 (0.1)	2.0 (3.7)	2.0 (3.7)
1C0.01MAX − TYPE3	0.0 (0.2)	3.5 (4.3)	3.5 (4.3)	0.0 (0.1)	2.3 (3.9)	2.3 (3.9)
2C0.5RAN − TYPE3	0.1 (0.2)	3.5 (4.6)	3.6 (4.7)	0.1 (0.2)	3.0 (4.4)	3.1 (4.5)
2C0.01RAN − TYPE3	0.2 (0.4)	3.6 (4.6)	3.8 (4.8)	0.2 (0.4)	3.3 (4.5)	3.5 (4.7)
2C0.5MAX − TYPE3	0.1 (0.2)	4.6 (5.5)	4.7 (5.6)	0.1 (0.2)	3.9 (5.3)	4.0 (5.4)
2C0.01MAX − TYPE3	0.2 (0.4)	4.9 (5.7)	5.1 (5.8)	0.2 (0.4)	4.4 (5.6)	4.6 (5.8)
NCRAN − TYPE3	−10.2 (12.1)	5.1 (5.4)	−5.1 (9.5)	−9.2 (11.9)	4.6 (5.3)	−4.6 (9.2)
NCMAX − TYPE3	−15.0 (14.8)	7.7 (7.2)	−7.3 (11.7)	−13.5 (14.8)	7.0 (7.2)	−6.5 (11.3)

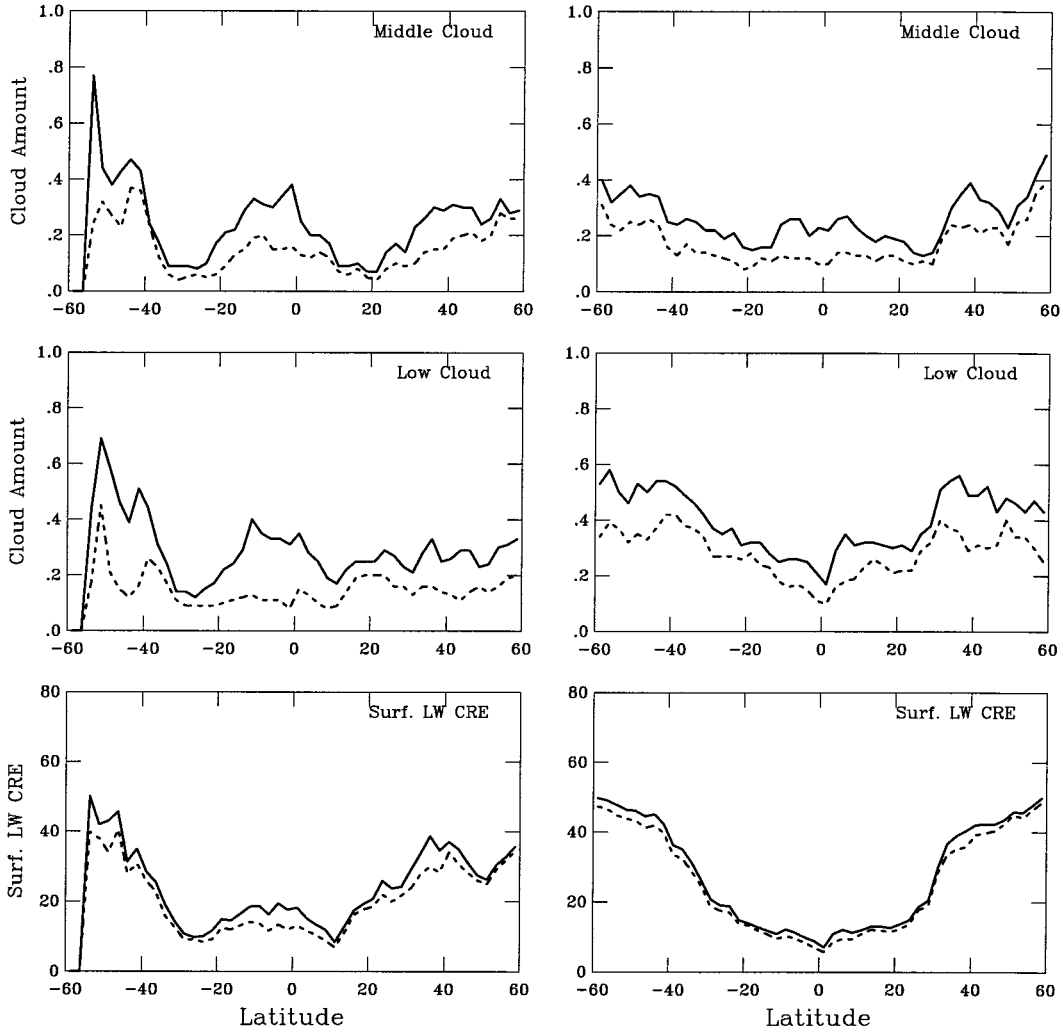

FIG. 5. Zonal averages of middle cloud amount (upper panels), low cloud amount (middle panels), and surface LW CRE (lower panels; W m^{-2}). Solid lines are for the overlap experiment 1C0.01MAX. Dashed lines are for the nonoverlap counterpart TYPE3. Left panels: over land. Right panels: over ocean. One day (15 Apr 1991) only.

TABLE 4. Same as Table 2 but in the atmosphere.

	Changed			All		
CRE in the atmosphere	SW	LW	TL	SW	LW	TL
TYPE9 − MEAN	—	—	—	0.3 (0.7)	0.3 (3.2)	0.6 (3.0)
TYPE3 − MEAN	—	—	—	0.1 (0.5)	0.6 (2.9)	0.7 (2.7)
1C0.5RAN − TYPE3	0.6 (0.9)	−4.0 (5.6)	−3.4 (4.9)	0.3 (0.7)	−2.4 (4.8)	−2.1 (4.2)
1C0.01RAN − TYPE3	0.7 (1.0)	−4.7 (6.5)	−4.0 (5.8)	0.5 (0.9)	−3.2 (5.9)	−2.7 (5.2)
1C0.5MAX − TYPE3	0.8 (1.0)	−5.7 (7.0)	−4.9 (6.2)	0.5 (0.9)	−3.5 (6.1)	−3.0 (5.4)
1C0.01MAX − TYPE3	0.9 (1.1)	−6.8 (8.2)	−5.9 (7.3)	0.6 (1.0)	−4.6 (7.4)	−4.0 (6.6)
2C0.5RAN − TYPE3	1.6 (2.2)	−10.3 (13.3)	−8.7 (11.4)	1.3 (2.1)	−8.7 (12.7)	−7.4 (10.9)
2C0.01RAN − TYPE3	1.8 (2.5)	−13.0 (16.6)	−11.2 (14.5)	1.6 (2.5)	−11.8 (16.3)	−10.2 (14.2)
2C0.5MAX − TYPE3	1.9 (2.3)	−12.9 (14.8)	−11.0 (12.9)	1.6 (2.2)	−11.0 (14.4)	−9.4 (12.6)
2C0.01MAX − TYPE3	2.2 (2.6)	−16.7 (18.7)	−14.5 (16.4)	2.0 (2.6)	−15.1 (18.4)	−13.1 (16.2)
NCRAN − TYPE3	0.3 (0.5)	−4.2 (4.7)	−3.9 (4.4)	0.3 (0.5)	−3.8 (4.6)	−3.5 (4.4)
NCMAX − TYPE3	0.4 (0.60)	−6.1 (6.2)	−5.7 (5.9)	0.4 (0.6)	−5.6 (6.2)	−5.2 (5.9)

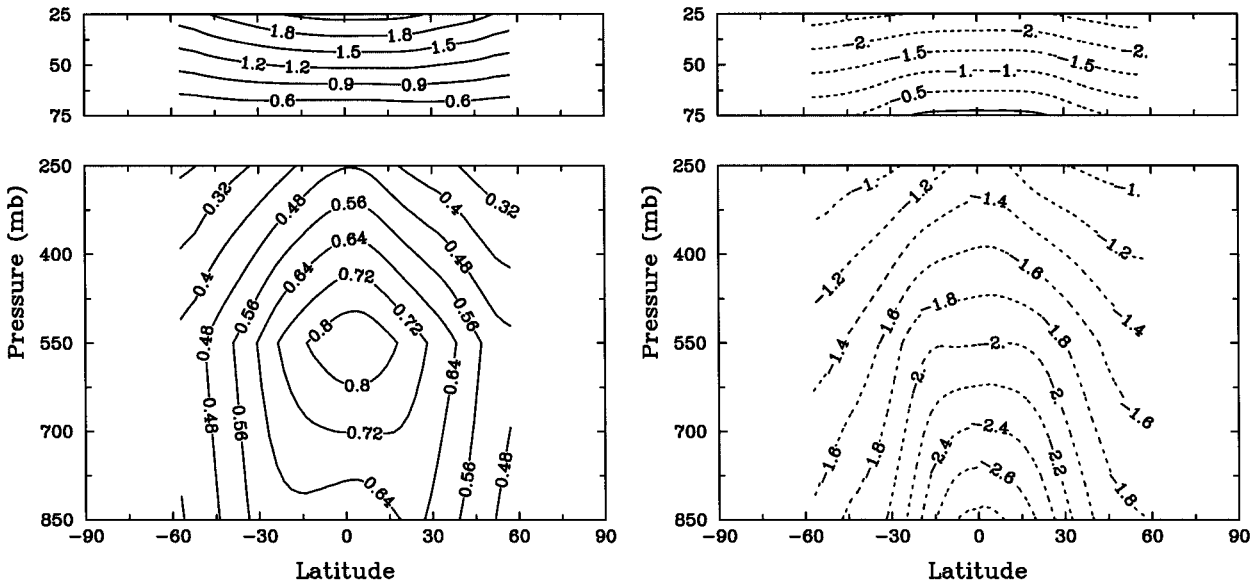

FIG. 6. Cross section of annual (4-day average), zonal average atmospheric radiative heating rates (K day^{-1}) for clear-sky conditions, all locations included. Left panels are for SW heating rates; right panels are for LW heating rates.

of lower-level cloudiness is increased, the in-atmosphere SW CRE increases to -0.8 W m^{-2} in NCRAN and 1.1 W m^{-2} in 2C0.01MAX from -1.1 W m^{-2} in the non-overlap counterpart (TYPE3). Rossow and Zhang (1995) found a global, annual mean value of -1.6 W m^{-2} by calculating the fluxes with a single average cloud layer. Although the small magnitude of the changes on average indicates that the SW absorption in the atmosphere is insensitive to the presence of clouds, local values of the CRE changes can exceed 10 W m^{-2}. Note that this result does not imply small cloud absorption of SW but arises from a cancellation between the increased SW absorption by the clouds together with the atmospheric layer above and the decreased absorption by the atmospheric layer below when clouds are present (Rossow and Zhang 1995). The increase of in-atmosphere SW CRE with τ-conserving overlap experiments can be explained by the same mechanisms discussed for TOA SW CRE. The increase of in-atmosphere SW CRE with no-constraint experiments arises primarily because more SW radiation is now reflected and absorbed by stratospheric ozone because of the increased reflectance from the added lower-level clouds. More detailed discussion of this issue is given in the next section, but, for now, it may be noted that the biggest change in the atmospheric column SW CRE is from one of the τ-conserving schemes, namely, constraint II. In other words, although the increase in lower-level cloud cover is larger when no constraint on optical thickness is applied, the overall effect on in-atmosphere SW CRE happens to be nearly zero. Note that we are treating the upper-level clouds as liquid water instead of ice, and correction for this error would change only slightly the quantitative results presented here.

The LW CRE in the atmosphere also balances two opposing effects (Rossow and Zhang 1995): adding clouds can reduce the overall emission temperature and LW flux, especially if they are at a higher level than the bulk of the water vapor, but also can increase the average emissivity (and the LW flux) of the atmosphere, especially in the water vapor window. The magnitudes of these two effects vary with the height of the cloud layers. Figure 4 and Table 4 show that, as cloud overlap is introduced in the various experiments, the global mean in-atmosphere LW CRE decreases (increased cooling) by amounts ranging from 4.0 W m^{-2} (2.4 W m^{-2}) in 1C0.5RAN to 16.7 W m^{-2} (15.1 W m^{-2}) in 2C0.01MAX for changed (all) locations. For the τ-conserving overlap experiments, this effect is caused by the progressive shift of the center of cloud mass to lower altitudes where the temperature is higher, leading to increased LW emission by the atmosphere at TOA and decreased LW absorption from the surface. For the no-constraint experiments, the enhanced LW cooling is due to the increased LW emission from adding extra relatively warm low-level clouds. Again the biggest changes in the atmospheric LW CRE are from the constraint-II experiments, not the experiments without a constraint on optical thickness applied.

4. Effect of cloud layer overlap on atmospheric radiative heating profiles

The in-atmosphere CRE shown in the previous section is the vertical integral over the whole atmosphere of the cloud-induced changes of the vertical radiative flux divergence. Radiative heating drives the atmospheric circulation through horizontal and vertical gra-

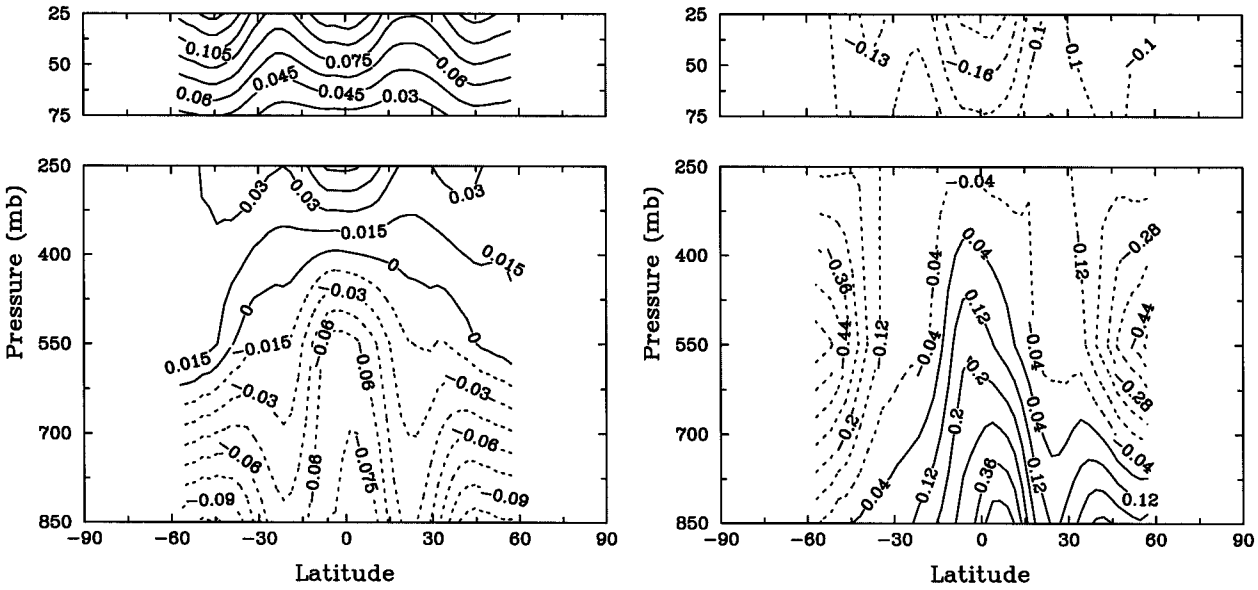

FIG. 7. Cross section of annual (4-day average), zonal average CRE on atmospheric radiative heating rates (K day^{-1}) for single-layer, nonoverlap experiment (MEAN), all locations included. Left panels are for SW heating rates; right panels are for LW heating rates.

dients of the volume radiative heating rate given by the flux divergences. In this section, we consider the effects of varying cloud vertical structure on profiles of radiative heating rate (vertical flux divergence) and their variation with latitude.

As a reference, Fig. 6 shows the 4-day and zonally averaged SW and LW heating profiles for clear-sky conditions.[5] Troposphere (surface to 100 mb) and stratosphere (100 mb and above) are presented separately. Several features are notable. 1) The SW heating rate peaks at midtropospheric levels near the equator (about 0.8 K day^{-1}) (Chapman profile; Wallace and Hobbs 1977). The pronounced hemispheric asymmetry in the SW heating profile, particularly near the surface, is caused by the larger annual mean humidity (associated with the warmer annual mean surface temperature) and surface albedo in the Northern than in the Southern Hemisphere. There is another peak of SW heating near 25 mb from ozone (more than 2 K day^{-1}) that is largely balanced by LW cooling throughout much of the stratosphere produced primarily by LW emission by carbon dioxide and ozone. 2) Strong LW cooling (about 3 K day^{-1}) occurs near the equatorial surface, consistent with the presence of the highest temperature and humidity. Very weak LW heating appears in the tropical lower stratosphere, where carbon dioxide and ozone absorb LW radiation from the warmer troposphere (Freeman and Liou 1979). 3) LW cooling dominates over SW heating throughout the troposphere, being strongest at the surface near the equator and decreasing with both latitude and altitude. Thus, for clear-sky conditions with the temperatures established in the current (cloudy) climate, the vertical gradient of radiative heating rate tends to stabilize the troposphere (stronger cooling at lower altitudes), and the horizontal gradient tends to decrease the forcing for the mean circulation (stronger cooling at lower latitudes).

Figure 7 displays the 4-day-averaged CRE on the SW and LW heating profiles (defined as the difference between the full-sky radiative heating profiles and the clear-sky radiative heating profiles) by calculating the flux divergence with a single average cloud layer as done by Zhang et al. (1995) (MEAN). For shortwave radiation, clouds, as a reflector for the atmospheric layer above and a shelter for the atmospheric layer below, slightly decrease the SW heating of the lower part of troposphere and increase the SW heating of the upper part of troposphere and stratosphere and, hence, tend to stabilize the atmosphere. For longwave radiation, clouds slightly reduce the cooling of the tropical lower and middle troposphere and the lower troposphere of midlatitudes in the Northern Hemisphere, because the clouds in these regions are generally higher than the bulk of the water vapor, causing a reduced overall emission temperature. In the dry, high latitudes, clouds enhance the LW cooling at all atmospheric levels (with peaks in the midtroposphere) because of increased average emissivity of the atmosphere, especially in the

[5] The contours in Figs. 6–12 are plotted using 300-mb resolution in the troposphere (because ISCCP reports clouds in three pressure categories) and 50-mb resolution in the stratosphere. Also, to smooth the contours, a uniform 5-point moving average is applied in the horizontal direction, leading to an effective resolution of 12.5° latitude. Note that the magnitude of the heating rates depends on the vertical and latitudinal resolutions. No calculations are reported beyond 57.5°S to 57.5°N latitudinal bands, because of the lack of wintertime optical thickness values.

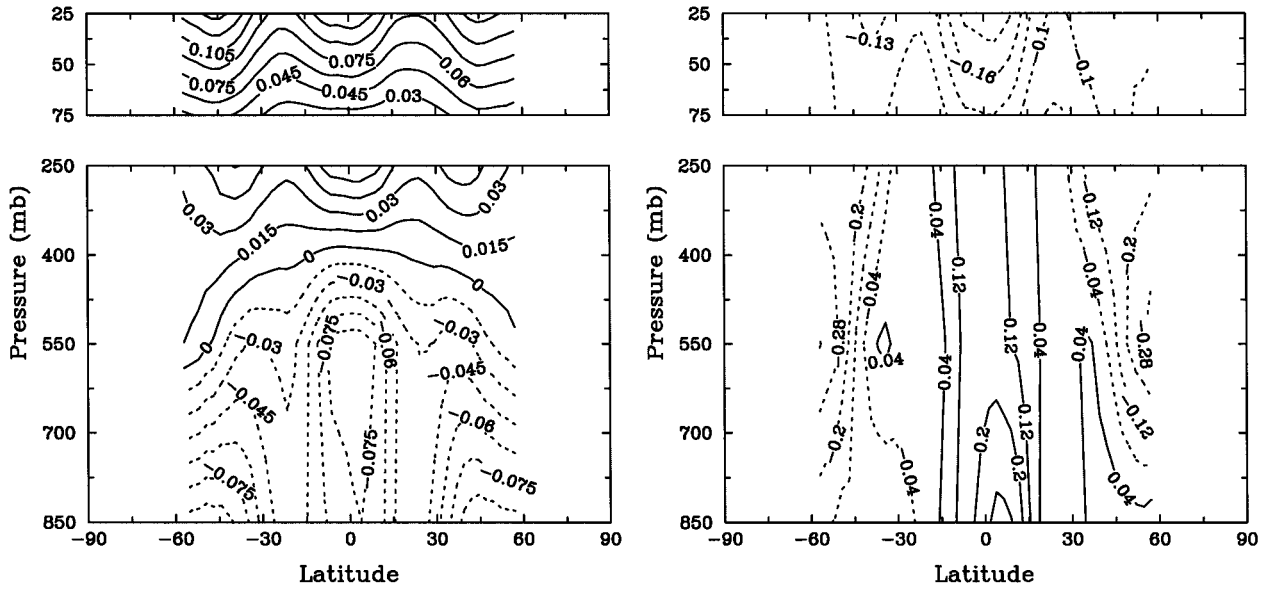

FIG. 8. Same as Fig. 7 but for three-layer, nonoverlap experiment (TYPE3).

water vapor window. The hemispheric asymmetry arises from the larger annual mean humidity in the Northern than in the Southern Hemisphere. Clouds also increase the LW cooling of the stratosphere by blocking the LW radiation from the surface. Overall, in the single-average-cloud-layer experiment (MEAN), clouds change the radiative cooling rate of the atmosphere by about 10%–30%, acting to decrease the stability of the tropical troposphere and the lower troposphere at higher latitudes but increasing the stability of the upper troposphere at higher latitudes.

Preaveraging the cloud types into one mean cloud has the consequence of shifting the clouds into the middle of the troposphere, similar to the SL4 experiment in Wang and Rossow (1998). Because the radiative profiles are particularly sensitive to the location of cloud layers, and because calculating the radiative heating rate with a single average cloud layer is undoubtedly an oversimplified approach, however, it is interesting to examine the CRE on radiative heating profiles calculated with three cloud layers but no overlap (TYPE3), shown in Fig. 8. In comparison with Fig. 7, the most striking feature is the different pattern of CRE on the LW heating profile; the vertical gradient is diminished considerably, implying that clouds (in the three-layer treatment) have little influence on the static stability of the tropical troposphere. This implication is understood readily by considering that the vertical distribution of clouds is more uniform in the TYPE3 experiment than in the MEAN experiment. The differences of CRE on radiative heating profiles between TYPE3 and MEAN are shown in Fig. 9. To highlight the differences, unchanged locations are excluded. This figure clearly shows that most of the differences arise in the longwave. Preaveraging the cloud types into one mean cloud (MEAN) tends to underestimate the LW cooling of the lower troposphere and overestimate the LW cooling of the upper troposphere, resulting in a more unstable troposphere in comparison with the three-cloud-layer treatment (TYPE3). Thus, although the single-layer, nonoverlapping treatment (MEAN) is capable of accurately estimating the overall cloud-induced radiative flux changes at TOA and the surface (Chen et al. 2000), it introduces systematic and significant errors in CRE on radiative heating rate profiles.

The effects of varying cloud vertical structure on the radiative heating profiles are illustrated in Figs. 10–12 as the differences in the 4-day, zonally averaged radiative heating profiles between three overlap experiments (1C0.5RAN representing the constraint-I schemes, 2C0.5RAN representing the constraint-II schemes, and NCRAN representing the no-constraint schemes) and the nonoverlap counterpart (TYPE3) (same as in Fig. 9; locations where there are no changes in the cloud layer structure are excluded). The following conclusions can be drawn from these figures.

a. Shortwave heating rate profile

Figure 10 (left) shows the changes in zonal mean shortwave heating rate for overlap experiment 1C0.5RAN. Increases of up to 0.03 K day^{-1} (roughly 5% of mean value for the SW heating rate) are found in the mid- and lower troposphere from the increase of the number of photons reaching there as the upper-level cloud optical thicknesses are reduced. The upper troposphere shows a comparable magnitude decrease in the zonal mean shortwave absorption as the number of absorbers (cloud mass) is reduced, but in a shallower layer, however, leading to a net increase in SW absorp-

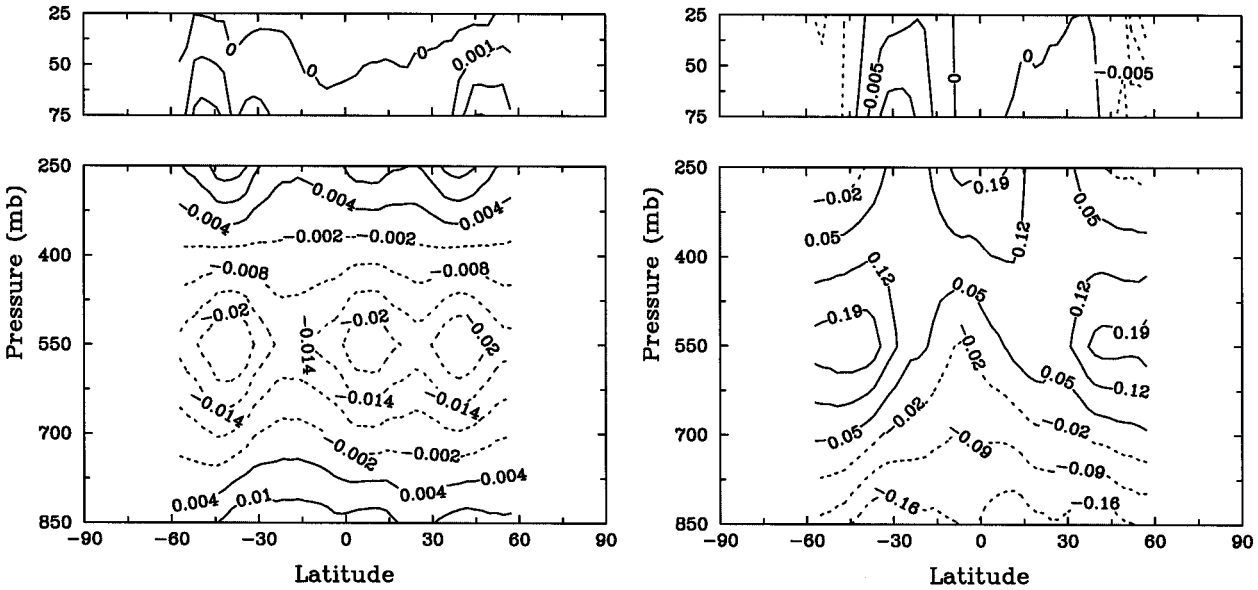

FIG. 9. Difference of CRE on atmospheric radiative heating rates (K day^{-1}) between experiment TYPE3 and experiment MEAN (TYPE3 minus MEAN; 4-day average), unchanged locations excluded; (left) SW; (right) LW.

tion for the entire atmospheric column as discussed in section 3. The overall pattern of the changes in zonal mean shortwave heating rate (Fig. 11; left) for the overlap experiment 2C0.5RAN is the same as that for 1C0.5RAN, for the same reasons, but the magnitudes are larger. Both results indicate that introducing cloud overlap in the τ-conserving experiments changes the SW heating so as to destabilize the atmosphere. The pattern of the zonal mean SW heating rate change is very different for the unconstrained overlap experiment (NCRAN; Fig. 12; left) with decreases up to 0.01 K day^{-1} in the lower troposphere and similar magnitude increases in the mid- and upper troposphere. The most notable changes in the SW heating rate appear in the stratosphere, however, with increases up to 0.02 K day^{-1}. The decrease of SW heating rate in the lower troposphere is simply the result of fewer photons reaching the lower troposphere because of increased low and middle cloud cover with the optical thickness of upper-level clouds unchanged. Similarly, the increase of SW heating in the mid- and upper troposphere as well as the stratosphere arises from the increased total reflec-

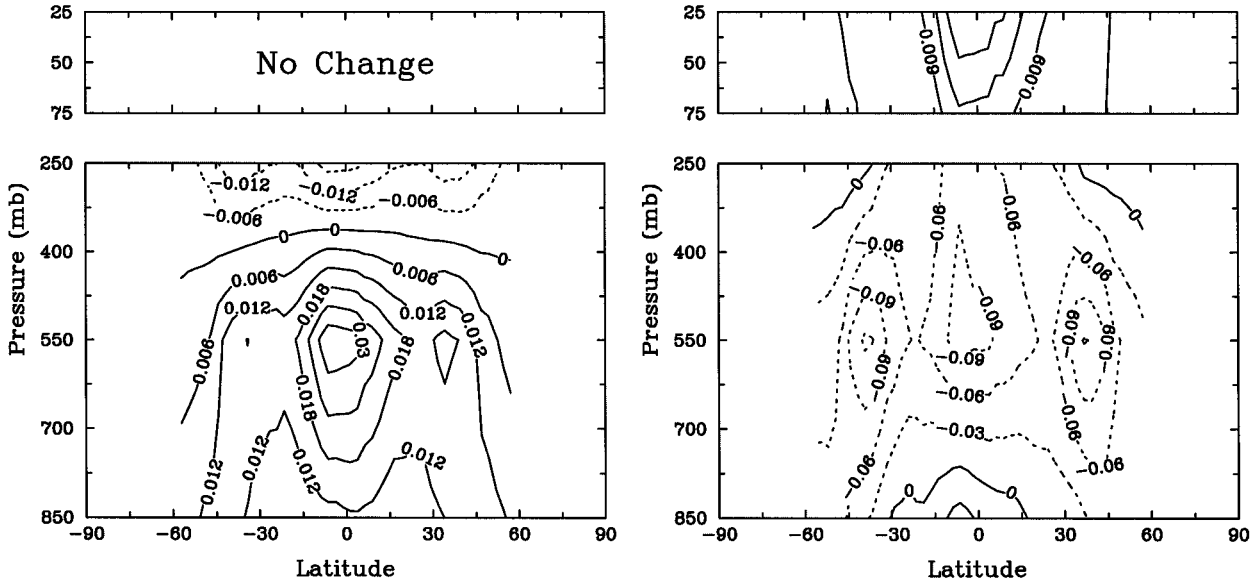

FIG. 10. Difference of CRE on atmospheric radiative heating rates (K day^{-1}) between overlap experiment 1C0.5RAN and three-layer, nonoverlap experiment TYPE3 (1C0.5RAN minus TYPE3; 4-day average), unchanged locations excluded. (left) SW; (right) LW.

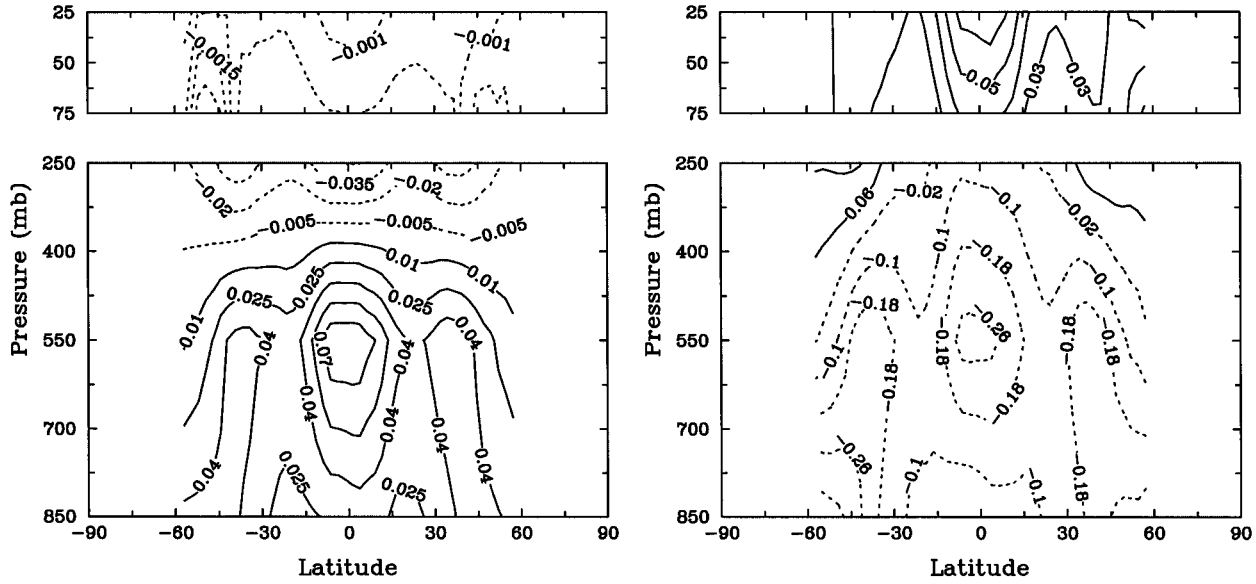

FIG. 11. Same as Fig. 10 but for 2C0.5RAN minus TYPE3.

tance as extra cloud mass is put into the atmosphere. Thus, introducing cloud overlap with no constraint on total cloud optical thickness tends to stabilize the atmosphere, as opposed to the effect of the τ-conserving experiments. Furthermore, in the stratosphere, the τ-conserving experiments hardly alter the SW heating, whereas the no-constraint experiments cause notable changes, because increased cloud reflectivity enhances SW absorption by stratospheric ozone. This effect can have consequences for stratospheric chemical processes. These results serve to illustrate the importance of the optical thickness constraint provided by the ISCCP dataset.

b. Longwave heating rate profile

Figure 10 (right) shows that, in comparison with the nonoverlap experiment (TYPE3), the overlap experiment 1C0.5RAN slightly reduces the longwave cooling near the tropical surface, in the upper troposphere at higher latitudes, and in the stratosphere but enhances the longwave cooling by up to 0.1 K day^{-1} in other regions. Figure 11 (right) shows a similar pattern for the overlap experiment 2C0.5RAN but with a larger magnitude (longwave cooling in the midtroposphere is increased up to 0.3 K day^{-1}). Notably, the reduced longwave cooling near the tropical surface, seen in Fig. 10,

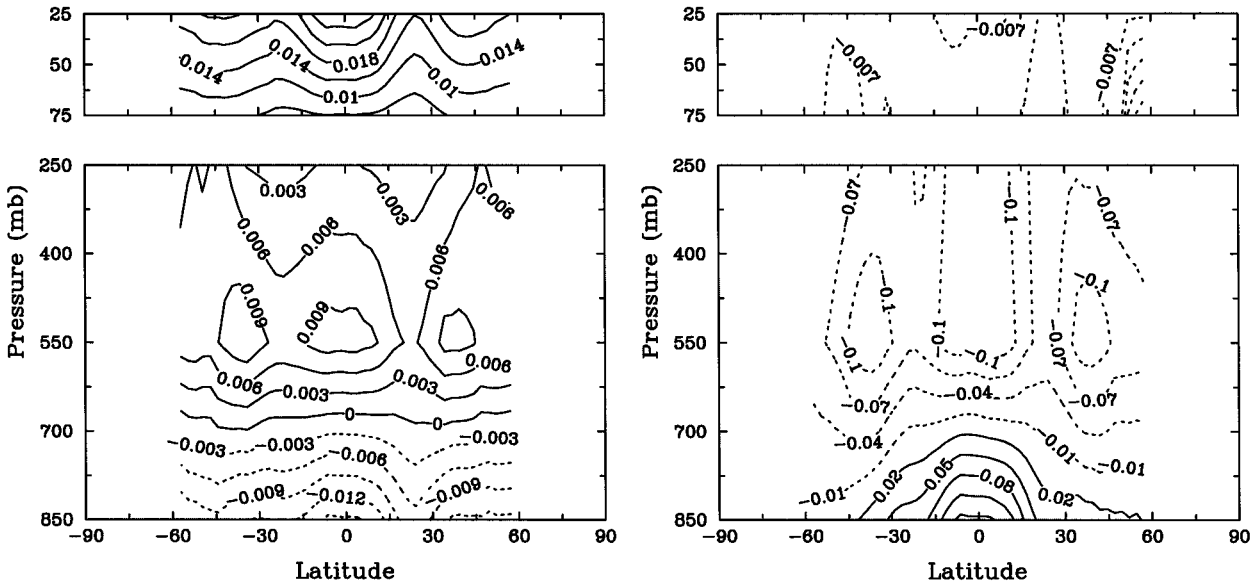

FIG. 12. Same as Fig. 10 but for NCRAN minus TYPE3.

is no longer present in Fig. 11. Although these differences are only 5%–10% of the clear-sky cooling rates (Fig. 6), they are of the same magnitude as the total LW CRE and are, thus, very significant. Because, in the τ-conserving experiments (e.g., 1C0.5RAN and 2C0.5RAN), moving part of the higher-level cloud mass to lower levels is equivalent to thinning the high-level clouds while inserting the low-level clouds, the changes can be explained by considering the following two LW effects. 1) Thinning high-level clouds cools the atmospheric layer below and heats the atmospheric layer above the clouds. The magnitude of this effect varies with cloud height and latitude because of variations in humidity. 2) Inserting low-level clouds heats the atmospheric layer below and cools the atmospheric layer above the clouds (cf. Ackerman et al. 1988). The differences in Figs. 10 (right) and 11 (right) arise from the relative importance of these two effects. Figure 12 (right) shows the LW heating rate change in the unconstrained overlap experiment (NCRAN) relative to the nonoverlap counterpart TYPE3; the longwave cooling of the lower tropical troposphere is decreased by up to 0.15 K day^{-1}, while the longwave cooling of the mid- and upper troposphere is increased by up to 0.1 K day^{-1}, resulting in a destabilizing effect. This result can be explained by the second effect mentioned above.

5. Conclusions

Several versions of three different cloud overlap schemes (constraint I, constraint II, and no constraint) used to infer cloud layer overlap for calculations of radiative fluxes and heating rate profiles with satellite-observed cloud fields are tested by determining the instantaneous radiative effects. The largest change (a reduction) in the SW absorption at TOA is produced by the unrealistic no constraint experiments, which do not conserve the vertically integrated cloud optical thickness that is observed. Constraint-II experiments are τ-conserving but still somewhat unrealistic, because the upper-level clouds are made too optically thin because of the small $\tau_{\text{threshold}}$ values used; they show the greatest increase in the LW radiation loss at TOA. At the surface, the no-constraint experiments cause the largest changes in both the SW and LW radiation budget, decreasing the surface SW absorption and increasing the surface LW absorption. The former effect exceeds the latter one, leading to an overall decrease in the total (SW plus LW) surface radiative heating. The τ-conserving experiments show the opposite change. For both the net SW and LW radiative fluxes in the atmosphere, the largest changes are produced in the constraint-II experiments. Thus, different overlap schemes exert very different influences on the radiation budget for different parts of the atmosphere–surface system. For all three overlap schemes, the magnitude of the radiative flux changes at TOA and SRF is relatively small, confirming the accuracy of the single-layer, nonoverlapping treatment used in the estimation of the TOA and SRF radiative fluxes, for example, by Zhang et al. (1995): errors caused by neglecting cloud layer overlaps are less than 2 W m^{-2} for SW and less than 15 W m^{-2} for LW.

For the most realistic scheme, constraint I, the changes in the TOA and SRF radiative fluxes are even smaller, even for estimating CRE at TOA and SRF. These global mean results do not preclude significant regional changes, however. Moreover, because the variations of cloud vertical structure are systematic with weather and climate regimes, these small errors are systematic and, consequently, ultimately cannot be ignored in evaluating the effects of cloud–radiation interactions on the climate.

The atmospheric radiative heating rate profiles are much more sensitive to uncertainties associated with unknown cloud layer overlaps. The nature of the effects varies with the overlap scheme used; the largest changes are produced by the constraint-II experiments and the smallest by the constraint-I experiments. Although the changes in both SW and LW heating rates are, in general, only about 10% of the mean clear-sky SW and LW heating rates, they are of comparable magnitude to the total SW and LW CRE on heating rates calculated with a nonoverlapping treatment (MEAN and TYPE3). Thus, unless information on the cloud vertical structure is available, one cannot accurately estimate CRE on the radiative heating rate profiles. More important, the τ-conserving experiments produce opposite-signed changes in the profile of atmospheric radiative heating rate (as well as fluxes, except for the SRF LW flux) in comparison with the schemes without conservation of total optical thickness, demonstrating the importance of conserving the total cloud optical thickness when applying any overlap assumption to satellite observations.

One limitation of these simple overlap schemes is that the satellite does not see lower levels as frequently as is needed to detect the presence of lower-level clouds. Moreover, because some meteorological situations produce *correlated* cloud layers (cf. Warren et al. 1985; Wang et al. 2000), instantaneous observations do not provide enough of a sample to use a statistical overlap rule. Thus, we need a more deterministic scheme that associates the satellite-observed cloud properties with particular cloud vertical structures, as might be obtained from a combination of ISCCP and a climatology of cloud vertical structure from rawinsonde humidity profiles (Wang et al. 2000).

This study has tested only the sensitivity of the radiative heating rate profiles to specified changes of cloud overlap. When the radiation and atmospheric dynamics interact, particularly when clouds are produced, a complete cloud feedback process results that may change the sensitivities presented here (cf. Wang and Rossow 1998; Ho et al. 1998). This issue is the critical one for climate research.

Acknowledgments. This study was suggested by un-

published studies of cloud layer overlap assumption on calculated surface longwave fluxes and longwave cooling rate profiles of the atmosphere for the international Surface Radiation Budget project. We benefited from conversations with G. L. Stephens and C. Stubenrauch. We thank both reviewers for their valuable comments and suggestions. This work is supported by the NASA Radiation and Climate Program, managed by Dr. Robert Curran, and NSF Grant 9629237.

REFERENCES

Ackerman, T. P., K. N. Liou, F. P. J. Valero, and L. Pfister, 1988: Heating rates in tropical anvils. *J. Atmos. Sci.,* **45,** 1606–1623.

Barkstrom, B. R., 1984: The Earth Radiation Budget Experiment (ERBE). *Bull. Amer. Meteor. Soc.,* **65,** 1170–1185.

Baum, B. A., B. A. Wielicki, P. Minnis, and S. C. Tsay, 1994: Multilevel cloud retrieval using multispectral HIRS and AVHRR data: Nighttime oceanic analysis. *J. Geophys. Res.,* **99,** 5499–5514.

Chen, T., W. B. Rossow, and Y.-C. Zhang, 2000: Radiative effects of cloud-type variations. *J. Climate,* **13,** 264–286.

Darnell, W. L., W. F. Staylor, S. K. Gupta, N. A. Ritchey, and A. C. Wilber, 1992: Seasonal variation of surface radiation budget derived from International Satellite Cloud Climatology Project C1 data. *J. Geophys. Res.,* **97,** 15 741–15 760.

Freeman, K. P., and K. N. Liou, 1979: Climate effects of cirrus clouds. *Advances in Geophysics,* Vol. 21, Academic Press, 231–287.

Fu, Q., K. N. Liou, M. C. Cribb, T. P. Charlock, and A. Grossman, 1997: Multiple scattering parameterization in thermal infrared radiative transfer. *J. Atmos. Sci.,* **54,** 2799–2812.

Hansen, J. E., G. Russel, D. Rind, P. Stone, A. A. Lacis, S. Lebedeff, R. Ruedy, and L. Travis, 1983: Efficient three-dimensional global models for climate studies: Models I and II. *Mon. Wea. Rev.,* **111,** 609–662.

Harrison, E. F., P. Minnis, B. R. Barkstrom, V. Ramanathan, R. D. Cess, and G. G. Gibson, 1990: Seasonal variation of cloud radiative forcing derived from the Earth Radiation Budget Experiment. *J. Geophys. Res.,* **95,** 18 687–18 703.

Hartmann, D. L., M. E. Ockert-Bell, and M. L. Michelsen, 1992: The effect of cloud type on Earth's energy balance: Global analysis. *J. Climate,* **5,** 1281–1304.

Ho, C.-H., M.-D. Chou, M. Suarez, and K.-M. Lau, 1998: Effect of ice cloud on GCM climate simulations. *Geophys. Res. Lett.,* **25,** 71–74.

Jin, Y., and W. B. Rossow, 1997: Detection of cirrus overlapping low-level clouds. *J. Geophys. Res.,* **102,** 1727–1737.

——, ——, and D. P. Wylie, 1996: Comparison of the climatologies of high-level clouds from HIRS and ISCCP. *J. Climate,* **9,** 2850–2879.

Kuhn, W. R., 1978: The effects of cloud height, thickness, and overlap on tropospheric terrestrial radiation. *J. Geophys. Res.,* **83,** 1337–1346.

Liang, X.-Z., and W.-C. Wang, 1997: Cloud overlap effects on general circulation model climate simulations. *J. Geophys. Res.,* **102,** 11 039–11 047.

Liao, X., W. B. Rossow, and D. Rind, 1995a: Comparison between SAGE II and ISCCP high-level clouds, 1. Global and zonal mean cloud amounts. *J. Geophys. Res.,* **100,** 1121–1135.

——, ——, and ——, 1995b: Comparison between SAGE II and ISCCP high-level clouds, 2. Locating cloud tops. *J. Geophys. Res.,* **100,** 1137–1147.

Liou, K. N., 1986: Influence of cirrus clouds on weather and climate processes: A global perspective. *Mon. Wea. Rev.,* **114,** 1167–1199.

Minnis, P., P. W. Heck, and D. F. Young, 1993: Inference of cirrus cloud properties using satellite-observed visible and infrared radiances. Part II: Verification of theoretical cirrus radiative properties. *J. Atmos. Sci.,* **50,** 1305–1322.

Mishchenko, M. I., W. B. Rossow, A. Macke, and A. A. Lacis, 1996: Sensitivity of cirrus cloud albedo, bidirectional reflectance and optical thickness retrieval accuracy to ice particle shape. *J. Geophys. Res.,* **101,** 16 973–16 985.

Morcrette, J. J., and Y. Fouquart, 1986: The overlapping of cloud layers in shortwave radiation parameterizations. *J. Atmos. Sci.,* **43,** 321–328.

Ockert-Bell, M. E., and D. L. Hartmann, 1992: The effect of cloud type on Earth's energy balance: Results for selected regions. *J. Climate,* **5,** 1158–1171.

Poore, K. D., J.-H. Wang, and W. B. Rossow, 1995: Cloud layer thicknesses from a combination of surface and upper-air observations. *J. Climate,* **8,** 550–568.

Ramaswamy, V., and V. Ramanathan, 1989: Solar absorption by cirrus clouds and the maintenance of the tropical upper troposphere thermal structure. *J. Atmos. Sci.,* **46,** 2293–2310.

Randall, D. A., Harshvardhan, D. A. Dazlich, and T. G. Corsetti, 1989: Interactions among radiation, convection, and large-scale dynamics in a general circulation model. *J. Atmos. Sci.,* **46,** 1943–1970.

Ridout, J. A., and T. E. Rosmond, 1996: Global modeling of cloud radiative effects using ISCCP cloud data *J. Climate,* **9,** 1479–1496.

Rossow, W. B., and A. A. Lacis, 1990: Global, seasonal cloud variations from satellite radiance measurements. Part II: Cloud properties and radiative effects. *J. Climate,* **3,** 1204–1253.

——, and R. A. Schiffer, 1991: ISCCP cloud data products. *Bull. Amer. Meteor. Soc.,* **72,** 2–20.

——, and Y.-C. Zhang, 1995: Calculation of surface and top of atmosphere radiative fluxes from physical quantities based on ISCCP data sets, 2. Validation and first results. *J. Geophys. Res.,* **100,** 1167–1197.

——, A. W. Walker, and L. C. Garder, 1993: Comparison of ISCCP and other cloud amounts. *J. Climate,* **6,** 2394–2418.

——, ——, D. E. Beuschel, and M. D. Roiter, 1996: International Satellite Cloud Climatology Project (ISCCP) Documentation of New Cloud Datasets. WMO/TD 737, World Climate Research Programme, Geneva, Switzerland, 115 pp.

Slingo, A., and J. M. Slingo, 1988: The response of a general circulation model to cloud longwave radiative forcing. I: Introduction and initial experiments. *Quart. J. Roy. Meteor. Soc.,* **114,** 1027–1062.

Stubenrauch, C. J., A. D. Del Genio, and W. B. Rossow, 1997: Implementation of subgrid cloud vertical structure inside a GCM and its effect on the radiation budget. *J. Climate,* **10,** 273–287.

——, W. B. Rossow, F. Cheruy, A. Chedin, and V. A. Scott, 1999: Clouds as seen by satellite sounders (3I) and imagers (ISCCP). Part I: Evaluation of cloud parameters. *J. Climate,* **12,** 2189–2213.

Tian, L., and J. A. Curry, 1989: Cloud overlap statistics. *J. Geophys. Res.,* **94,** 9925–9935.

Toon, O. B., C. P. McKay, and T. P. Ackerman, 1989: Rapid calculation of radiative heating rates and photodissociation rates in inhomogeneous multiple scattering atmospheres. *J. Geophys. Res.,* **94,** 16 287–16 301.

Wallace, J. M., and P. V. Hobbs, 1977: *Atmospheric Science—An Introductory Survey.* Academic Press, 467 pp.

Wang, J.-H., 1997: Determination of cloud vertical structure from upper air observations and its effects on atmospheric circulation in a GCM. Ph.D. dissertation, Columbia University, 233 pp. [Available from Junhong Wang, NCAR/SSSF, P. O. Box 3000, Boulder, CO 80307.]

——, and W. B. Rossow, 1995: Determination of cloud vertical structure from upper-air observations. *J. Appl. Meteor.,* **34,** 2243–2258.

——, and ——, 1998: Effects of cloud vertical structure on atmospheric circulation in the GISS GCM. *J. Climate,* **11,** 3010–3029.

——, ——, and Y.-C. Zhang, 2000: Cloud vertical structure and its variations from a 20-yr global rawinsonde dataset. *J. Climate,* in press.

Warren, S. G., C. J. Hahn, and J. London, 1985: Simultaneous occurrence of different cloud types. *J. Climate Appl. Meteor.*, **24,** 658–667.

——, ——, R. M. Chervin, and R. L. Jenne, 1986: Global distribution of total cloud cover and cloud type amounts over land. NCAR Tech. Note NCAR/TN-273+STR, 29 pp. and 200 maps. [Available from National Center for Atmospheric Research, P.O. Box 3000, Boulder, CO 80307.]

——, ——, J. London, R. M. Chervin, and R. L. Jenne, 1988: Global distribution of total cloud cover and cloud type amounts over ocean. NCAR Tech. Note NCAR/TN-317+STR, 42 pp. and 170 maps. [Available from National Center for Atmospheric Research, P.O. Box 3000, Boulder, CO 80307.]

Zhang, Y.-C., W. B. Rossow, and A. A. Lacis, 1995: Calculation of surface and top of atmosphere radiative fluxes from physical quantities based on ISCCP data sets, 1. Method and sensitivity to input data uncertainties. *J. Geophys. Res.*, **100,** 1149–1165.